ACS OMEGA

http://pubs.acs.org/journal/acsodf

Article

Eco-Benign Orange-Hued Pigment Derived from Aluminum-Enriched Biogenous Iron Oxide Sheaths

Katsunori Tamura,* Yuri Oshima, Yuta Fuse, Noriyuki Nagaoka, Tatsuki Kunoh, Makoto Nakanishi, Tatsuo Fujii, Tokuro Nanba, and Jun Takada*

Cite This: *ACS Omega* 2022, 7, 12795−12802

Read Online

ACCESS | Metrics & More | Article Recommendations | Supporting Information

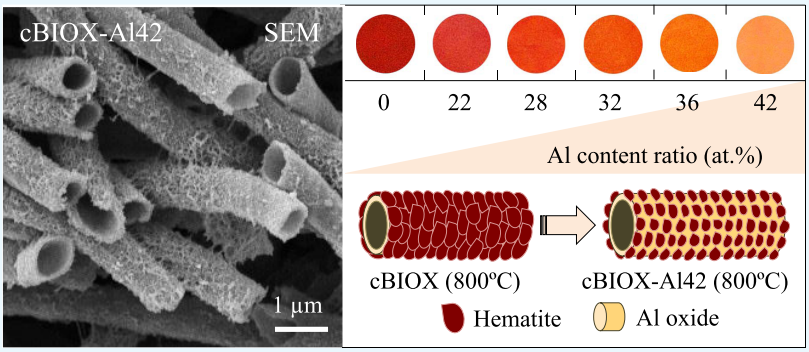

ABSTRACT: Inorganic pigments have been widely used due to their low cost of production, strong hiding power, and chemical resistance; nevertheless, they have limited hue width and chromaticity. To eliminate these disadvantages, we herein propose the use of an ingenious biotemplate technique to produce Al-enriched biogenic iron oxide (BIOX) materials. Spectrophotometric color analysis showed that high levels of Al inclusion on heat-treated BIOX samples produced heightened yellowish hues and lightness. The Al-enriched BIOX sheaths exhibited a stable tubular structure and excellent thermal stability of color tones after heating at high temperatures and repetitive heat treatments. Ultrastructural analysis and mechanical destruction experiments revealed that the highly chromatic orange-hue of these pigments are ascribed probably to an ingenious cylindrical nanocomposite architecture composed of putative Fe-included low crystalline Al oxide regions and hematite particles embedded therein. The present work therefore demonstrates that the bioengineered material can serve as an epochal orange-hued inorganic pigment with low toxicity and marked thermostability that should meet large industrial demand.

INTRODUCTION

Known from prehistoric times, inorganic pigments are key components in the production of a wide range of materials, due to their excellent properties, such as higher thermal stability, chemical resistance, and weather durability.[1] Despite these advantages, most inorganic pigments present a very narrow hue range and insufficient chroma, except those containing hazardous substances, such as lead compounds (Pb_3O_4, $PbCrO_4$), cadmium compounds (CdS, Cd_2SSe), chromium compounds ($ZnCrO_4$, $CaCrO_4$), and mercury(II) sulfide (HgS).[2] In the past two decades, stricter regulations have been put in place worldwide to minimize the environmental and health effects of hazardous substances. For example, the Strategic Approach to International Chemicals Management (SAICM)—adopted in 2006 at the International Conference on Chemicals Management—ensures that, by the end of 2020, chemicals will be produced and used in safer ways, without impacting the world.[3] In the European Union, since the REACH regulation was enacted in 2006, an increasing number of harmful substances are subject to restricted production, sale, and use.[4−6] In the United States, the Toxic Substances Control Act was amended in 2016 by the Frank R. Lautenberg Chemical Safety Act for the 21st Century to regulate the use of hazardous substances.[7,8] In Japan, new and existing substances are regulated by the Substances Control Law, amended in 2009.[9] Therefore, as high chroma inorganic pigments that comply with all of these regulations are limited, many studies have focused on alternative color materials with low toxicity.[10−13]

In ancient times, hematite pigments have been used for coloring murals and ornaments; nowadays, owing to their extremely low toxicity, wide availability, and high hiding power, these pigments are used for ceramics, cosmetics, exterior wall

Received: December 31, 2021
Accepted: March 22, 2022
Published: April 10, 2022

https://doi.org/10.1021/acsomega.1c07390
ACS Omega 2022, 7, 12795−12802

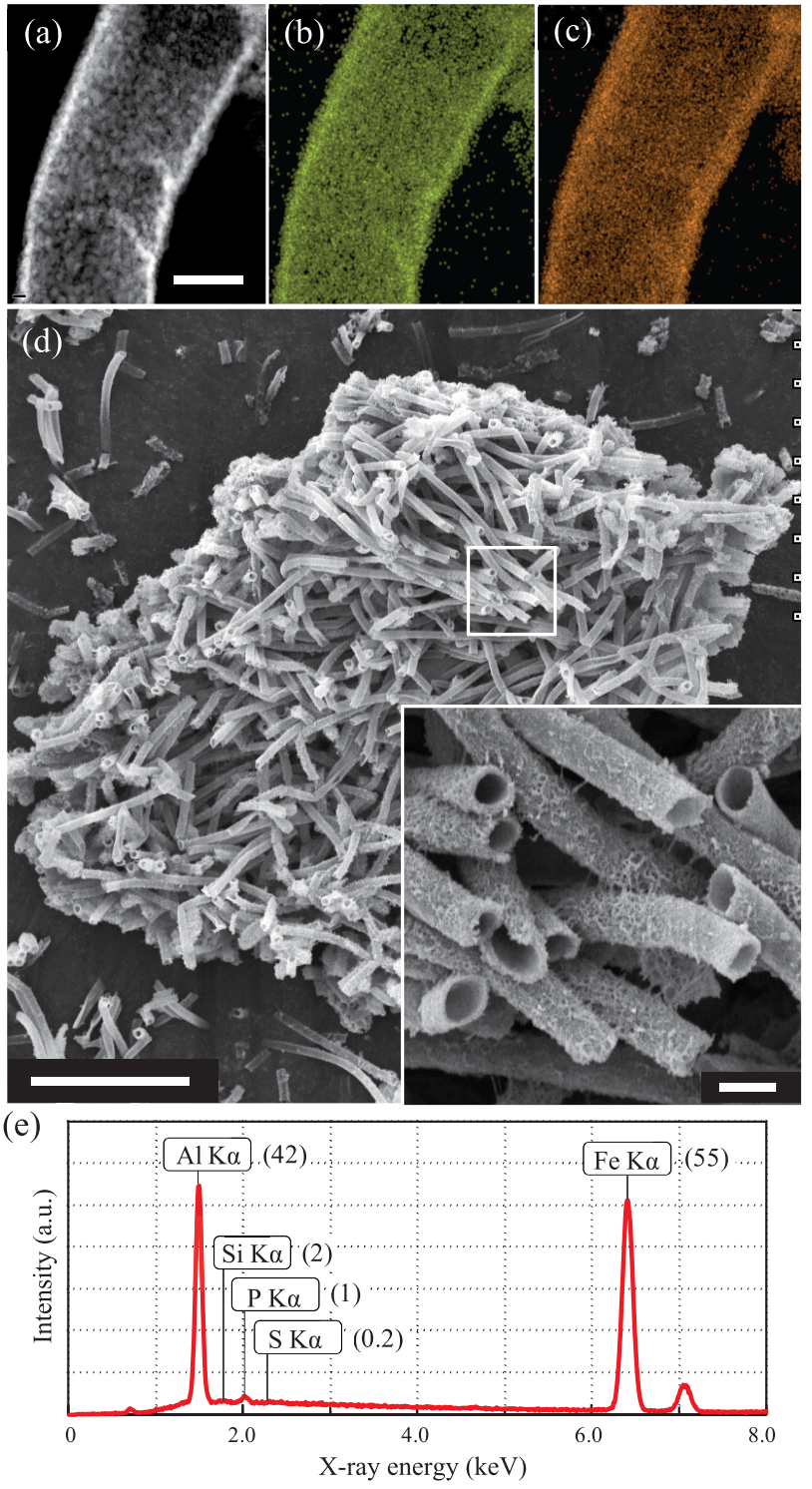

Figure 1. Morphology and chemical composition of the cBIOX-Al sample. (a) Dark-field STEM image of an as-prepared cBIOX-Al32 sheath before heating. The scale bar is 500 nm. (b, c) Elemental mapping images of (b) Fe K and (c) Al K edges obtained by EDS area analysis of the view in (a). (d) Scanning electron microscopy (SEM) image of a sheath clump of cBIOX-Al42 after heating at 800 °C; the inset shows a magnified image of the white square area. The scale bar is 20 μm (1 μm in inset). (e) XRF spectrum of cBIOX-Al42. Numerical values in parentheses are the respective composition ratios (atom %).

paintings, and road pavements.[1,2,14] Besides the mineral and chemical pathways of synthesizing iron oxides, the bioderived ones—biogenic iron oxide (BIOX)—are considered promising raw materials for highly thermostable inorganic red pigments.[15,16] Interestingly, the BIOXs can have different morphologies such as: (i) unique microtubular sheath with high porousness, (ii) organic−inorganic hybrid construct composed mainly of primary nanoparticles of amorphous ferric oxyhydroxides, or (iii) nanocomposite structures formed by sintering.[17,18] Recent studies have shown that the chemical compositions of the cultured BIOX (cBIOX) sheaths are modifiable by biotemplate techniques using isolated iron

https://doi.org/10.1021/acsomega.1c07390
ACS Omega 2022, 7, 12795−12802

bacterial strains.[19,20] Moreover, the additive elements deposited on the BIOX sheaths could readily improve the color tones in heated products, indicating that the BIOXs are easily tunable materials.[21] Herein, we describe new orange-hued iron oxide pigments with readily modifiable hues by changing the elemental composition in the BIOXs.

RESULTS AND DISCUSSION

Preparation and Physicochemical Characterization of Al-Enriched cBIOX Sheaths. The aim of this study was to improve the hue of heat-treated BIOX materials via modifying their chemical compositions. Previous studies have shown that the inclusion of Al in the chemically synthesized hematite-based pigments produced yellowish-red hues[22−24] and that the additive deposition of Al in BIOX-derived pigments resulted in an increased yellowish intensity.[21] Using a two-step method,[19] we have prepared highly enriched Al-containing cBIOX sheaths by the addition of 10 mM $AlCl_3$ solution over various concentrations of $ZnSO_4$. Tube-shaped sheaths of cBIOX were successfully obtained at low concentrations of $ZnSO_4$ (≤10 mM), while an excess of sulfate ions might hinder the formation of cBIOX. The morphology analysis showed that the sample prepared using the 10 mM $ZnSO_4$ solution is formed of hollow tubular sheaths, each tube having a size of 0.9−1.2 μm in outer diameter and dozens to hundreds of micrometers in length (Figure S1). The content ratio of Al present in the cBIOX products was determined using X-ray fluorescence (XRF) spectroscopy. The materials prepared using 2 and 10 mM $ZnSO_4$ solutions contained 24 and 32 atom %, respectively, hereafter referred to as cBIOX-Al24 and cBIOX-Al32 (Figure S1); the Al content ratio in the sample prepared in the absence of $ZnSO_4$ was 21 atom % (denoted cBIOX-Al21). These results clearly demonstrate that the presence of sulfate ions favors the deposition of Al on the cBIOX sheaths. Furthermore, the scanning transmission electron microscopy-energy-dispersive X-ray spectroscopy (STEM-EDS) analysis demonstrates that there is a uniform distribution of Al and Fe on the sheath body (Figure 1a−c).

Next, we have investigated the physicochemical features of the cBIOX-Al32 after heating at 800 °C, the temperature at which amorphous ferric oxyhydroxide changes to hematite.[25] The morphology analysis showed that the tubular shape of the sample was fully maintained along with a slight reduction in tube size (Figure 1d). Notably, XRF analysis revealed that the heat treatments caused a marked increase in the Al content ratio up to 42 atom % in the sample (hereafter referred to as cBIOX-Al42) in parallel with a dramatic decrease in the sulfur content ratio (Figures 1e and S1). We infer that the change in the elemental composition ratios after heating resulted probably from the release of sulfur oxides (SO_x), also reported by Perraud et al.[26] Besides, nitrogen adsorption isotherm analysis of cBIOX-Al42 showed relatively high specific surface area and microporosity (64.8 $m^2\ g^{-1}$, r_p = 1.2 nm for mesopores, d_p = 0.7 nm for micropores), which are probably favorable for the dispersibility when using as a pigment.

Behavior of Sulfate on cBIOX Sheaths. To explore the effect of sulfates on the increased Al content ratios in cBIOX sheaths, two materials were analyzed using thermogravimetry (TG): cBIOX-Al32 and cBIOX-Al21 prepared with and without $ZnSO_4$, respectively. Both materials presented a weight loss in the temperature range of 250−430 °C, probably due to the thermo-oxidative decomposition of the organic constituents. cBIOX-Al32 experienced an additional weight loss between 575 and 720 °C (Figure S2a), as a result of sulfur oxides emission via thermo-oxidation and vaporization.[27] Based on the results of TG analysis, the chemical compositions of cBIOX-Al32 heated at 500 and 700 °C were examined by XRF analysis. Figure 2a shows a drastic reduction in the sulfur

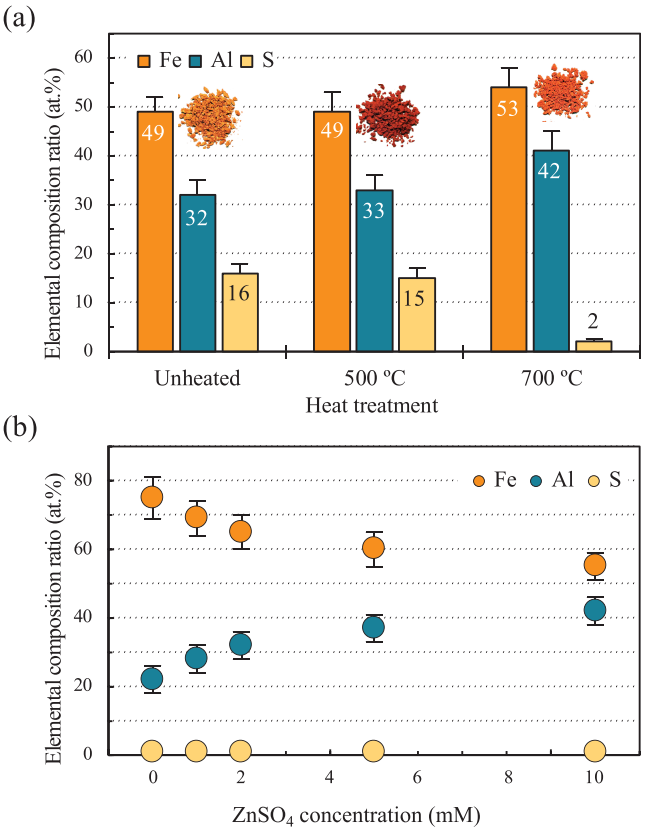

Figure 2. Analysis of the behavior of sulfate in cBIOX-Al samples. (a) Changes in elemental composition ratios before and after heating at 500 and 700 °C. Rectangular bars and vertical line bars represent mean ± SD (n = 10). Si (2 atom %) and P (1 atom %) are omitted because of almost constant values in every case. Powder images are shown above the bar chart. (b) Relationship between $ZnSO_4$ concentrations and elemental composition ratios in heat-treated cBIOX-Al samples. Plots and vertical bars represent mean ± SD (n = 10).

content ratio in relation to the increase in Fe and Al content ratios after heating at 700 °C, which were dissimilar to mostly unchanged chemical composition ratios in cBIOX-Al21 (data not shown). The loss of sulfates group in cBIOX-Al32 after heating at 800 °C was also proven by Fourier transform infrared (FTIR) spectroscopy (Figure S2b). We have also studied the effect of $ZnSO_4$ concentration on the Al content ratio in the cBIOX products. Figure 2b shows that, when the same concentration of Al precursor is used, the composition ratio of Al in the cBIOX increases with an increase in the zinc sulfate concentration; the findings were also verified by inductively coupled plasma-optical emission spectroscopy (ICP-OES) (Figure S2c). To understand if the cation has an effect on the Al deposition on the cBIOX, $(NH_4)_2SO_4$ and Na_2SO_4 were further used. The results demonstrate that the Al content ratio is dependent on the sulfate ions and not on the cations (Figure S2d). Although the mechanism behind this process is not totally understood, it is conceivable that the Al deposition in the cBIOX formation process was ascribed to the

https://doi.org/10.1021/acsomega.1c07390
ACS Omega 2022, 7, 12795−12802

relatively high ion-binding affinity between SO_4^{2-} and Al^{3+} as reported by Silva et al.[28] and Bennett et al.[29]

Colorimetric Characterization. The color characteristics of the Al-enriched cBIOX samples were evaluated after heating the materials at 800 °C in air. Figure 3a shows that the basic

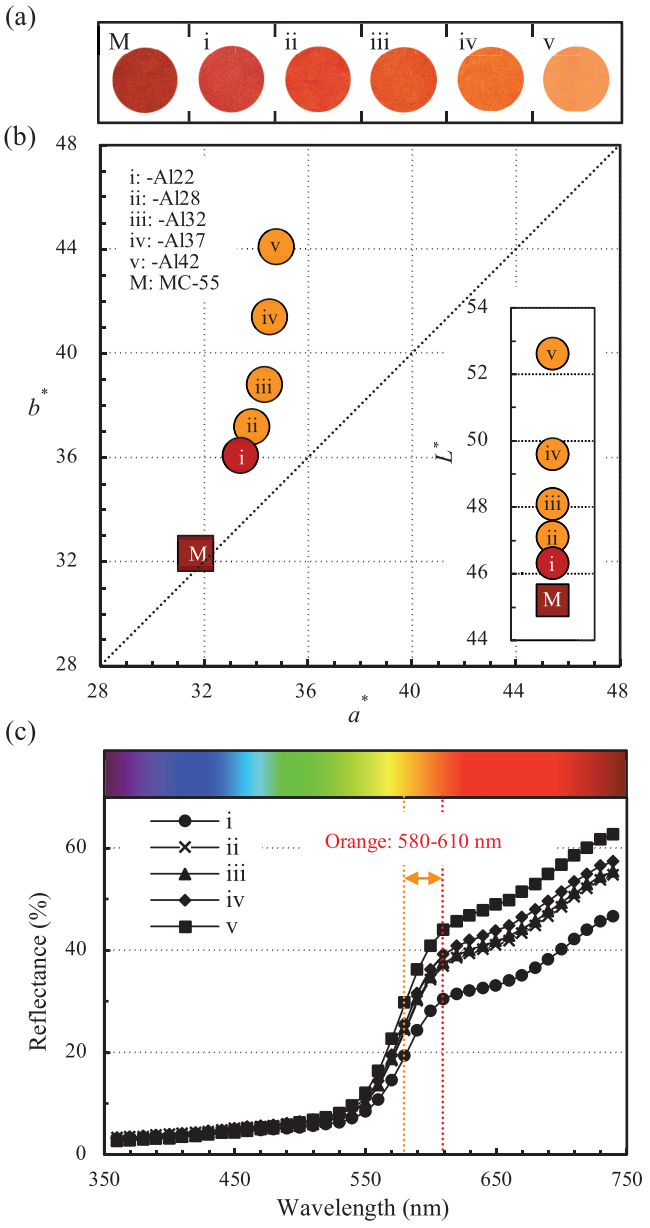

Figure 3. Color characteristics of heat-treated cBIOX-Al samples. (a) Powder images of (i) cBIOX-Al22, (ii) -Al28, (iii) -Al32, (iv) -Al37, and (v) -Al42. "M" indicates MC-55 used as the color reference. Photos were taken after stuffing the powder samples in cylindrical pits on glass plates. (b) CIE Lab coordinates for color tone values of cBIOX-Al samples. (c) Reflectance curves of cBIOX-Al samples.

reddish-brown hues of the powder samples turned to orange hues with the increase in the Al content ratio. Spectrophotometric color analysis revealed that the b^* values significantly increased with the increase in Al content ratios; in contrast, there was a slight increase of the a^* values on the color coordinates (Figure 3b, see Table S1 for details). It is thus unambiguous that the increase in Al/Fe ratios at the high levels led to the modification of hues. Likewise, the L^* values for lightness increased in the same manner as the other values. In the iron(III)-rich oxides such as hematite and spinel, the intense reddish-brown colors are attributed to the complete absorption light in high-energy regions of visible light (400−550 nm) and to the reflectivity in low-energy parts (550−800 nm).[30,31] In this regard, a comparison of the reflectance curves showed that the range of reflectance wavelengths widened with the increase in Al content ratios (Figure 3c), clearly proving that Al has a direct effect on hues. In general, the chromaticity of hematite-based pigments is affected by various factors including (i) crystal phase, (ii) crystallinity, (iii) crystallite size, (iv) solid solution of nonferrous elements, (v) composites, and (vi) grain boundary state.[1,14] Regardless of the Al content ratios in the cBIOX products, all materials presented a monophasic pattern of hematite with sufficient crystallinity in X-ray diffraction (XRD) images (Figure S3a). In addition, the grain growth of the hematite after the heat treatment was suppressed independently of Al content ratios (Figure 5e). On the other hand, no significant decrease in the lattice parameters of hematite was detected in the Al-enriched samples (Figure S3b), suggesting that the altered hues are not at least due to the change in lattice volume. In this connection, the Al substitution in hematite crystallites of the cBIOX-Al42 sample was estimated to be approximately 8 mol % by collating the lattice parameter values with the relevant data reported by Hashimoto et al.[24]

Thermostability of Color Tones. For practical purposes, we have studied the changes in color tones with temperature for the cBIOX-Al42 and cBIOX-Al22 samples. Figure 4a shows a relatively small difference in color values among the samples heated at various temperatures ranging from 700 to 1100 °C. Notably, the cBIOX-Al42 sample heated at 1000 and 1100 °C exhibited higher chroma and lightness compared to the case of cBIOX-Al22 (Figure 4a, Table S2). In addition, the cBIOX-Al42 sample maintained the high color values even after reheating at 800 °C (Figure 4b), shown by small degrees of color difference values ($\Delta L^* = -1.4$, $\Delta a^* = -0.8$, and $\Delta b^* = -0.8$, see Table S2). These results indicate that Al-enriched cBIOX possesses remarkable thermostability of color tones as the Al inclusion participates in the thermal stability of the hematite-based pigments.[21,23] The high thermal stability might be directly related to the suppression of the grain growth of the hematite in the cBIOX-Al42, as compared with the case of cBIOX-Al22 Figure 5e); moreover, the tubular shape of cBIOX-Al42 was maintained after heating at 1100 °C and reheating (Figure S1g,h). On the other hand, the mechanical destruction of the tubular structure by ball mill grindings after heating at 800 °C resulted in a significant decrease in chromaticity and lightness of cBIOX-Al42 (Figures 4b and S1i); in particular, the yellowish hue (b^*) diminished, as shown by the color difference values ($\Delta L^* = -9.0$, $\Delta a^* = -4.7$, and $\Delta b^* = -15.2$; see Table S2). The results suggest that the hollow cylindrical structure is somehow responsible for the orange-hued color tones observed in the intact cBIOX-Al42.

Microstructural Analysis of Thermostable Color Tones. To better understand the factors responsible for the altered hues and the improved color tones, we have studied the microstructures using ultrathin sections of cBIOX-Al42 sheaths. STEM-EDS mapping analysis showed distinct distributions of well-defined hematite particles and blurry regions of Al_2O_3 due to its poor crystallinity (Figure 5a−c). The EDS analysis showed Fe-specific signals in the Al oxide

https://doi.org/10.1021/acsomega.1c07390
ACS Omega 2022, 7, 12795−12802

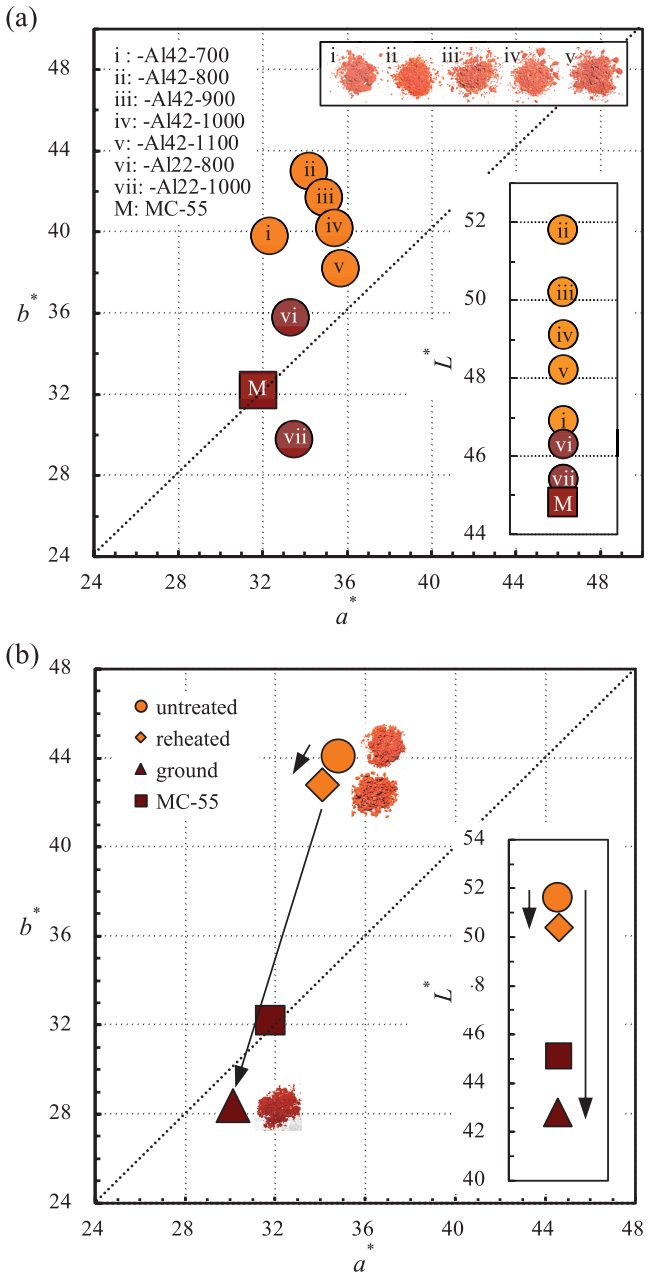

Figure 4. Analysis of thermostability in color tones of cBIOX-Al42. (a) CIE Lab coordinates for color tone values of cBIOX-Al samples after heating at the indicated temperatures (numerals after the second hyphen). Photos in the inset are powder images. (b) Changes in color tones of cBIOX-Al42 after reheating at 800 °C (reheated) or ball mill grinding (ground). Powder images are shown beside the plots. Arrows indicate directions and magnitudes of changes in color tones.

regions (Figure S4), and the XRD analysis revealed that the diffraction peaks of α-Al_2O_3 in the 1100 °C-heated cBIOX-Al42 shifted toward lower angles (Figure S3c). It was reported that approximately 10 mol % of Al in α-Al_2O_3 was substituted with iron when the material is heated at 1000 °C.[32] Therefore, the inclusion of ferric ions in Al oxides affected the phase transformation of Al_2O_3 during the sintering process, in agreement with Stößer et al.[33] Given that pure Al_2O_3 does not absorb visible lights and inclusions of impurities can affect the absorption,[34] it can be stated that the solid solution of Fe in Al oxide regions influences the visible light reflectivity of the materials. Furthermore, transmission electron microscopy (TEM) analysis revealed a distinct spatial distribution consisting of (i) particulate crystallites with high electron density corresponding to hematite and (ii) stippling pattern areas equivalent to putative Al oxides with poor crystallinity (Figure 5d). These results indicate the cylindrical nanocomposite structure of the sheath: low crystalline Fe-substituted Al oxide regions and hematite particles embedded in them, as shown in Figure 5f. Consequently, we argue that the low crystalline Al oxide regions are "optical modifiers" by altering light absorption properties with dose dependency and "stabilizing factors" by both preventing hematite grain growths and maintaining the cylindrical morphology during heat treatments. Incidentally, several lines of study have shown the low toxicity of Al oxides[35−38] as well as of hematite nanoparticles.[39]

Altogether, we have demonstrated that the bioengineering approach enabled us to produce Al-enriched iron oxide sheaths with the cylindrical nanocomposite structure and that the unprecedented cBIOX products can serve as high chromatic orange-hued pigments after heating, the hues of which are alterable by relatively simple expedient manipulations using sulfate additives. It is conceivable that the unique microtubular architecture probably contributes to the improved thermostable color tones through modifying optical properties such as light absorption, reflection, and transmission and preventing the grain growth of hematite during sintering. The BIOX-derived pigments have both excellent chromaticity and thermostability, suitable for ceramics, cosmetics, and paintings. Further, the stability of color tones in various solvents or detergent-containing water immersion is a forthcoming issue to be addressed toward the practical application. The biotemplate method has recently attracted much attention due to its prominent advantages in producing morphology-controlled materials with structural specificity, complexity, and unique functions.[40,41] Indeed, the biotemplating process of microbial origin used in this study led to the production of ingenious microtubular nanocomposite structures that are otherwise difficult to synthesize.

CONCLUSIONS

In the present study, we have shown unprecedented innoxious hematite-based pigments with altered hues prepared by discretionary adjustment of Al content ratios at high levels in the BIOX sheaths using a bioengineering approach. With the use of the two-step BIOX preparation method based on the biotemplate technique, highly Al-enriched BIOX products were obtained, in which the Al content ratios were optionally controllable depending on the concentrations of sulfate ions added to the metal deposition process. Spectrophotometric color analysis showed that high levels of Al inclusion on heat (800 °C)-treated BIOX samples caused heightened yellowish hues and lightness according to the increase in Al content ratios, which were closely connected with the reflected wavelength of visible light that widened to the short-wavelength side. The Al-enriched BIOX sheaths exhibited a stable tubular structure and excellent thermal stability of color tones after heating at high temperatures and repetitive heat treatments. Microstructural analysis and mechanical destruction experiments of the tubular structure revealed that the highly chromatic orange-hue of the Al-enriched BIOX materials are ascribed probably to an ingenious cylindrical nanocomposite architecture composed of putative Fe-included

https://doi.org/10.1021/acsomega.1c07390
ACS Omega 2022, 7, 12795−12802

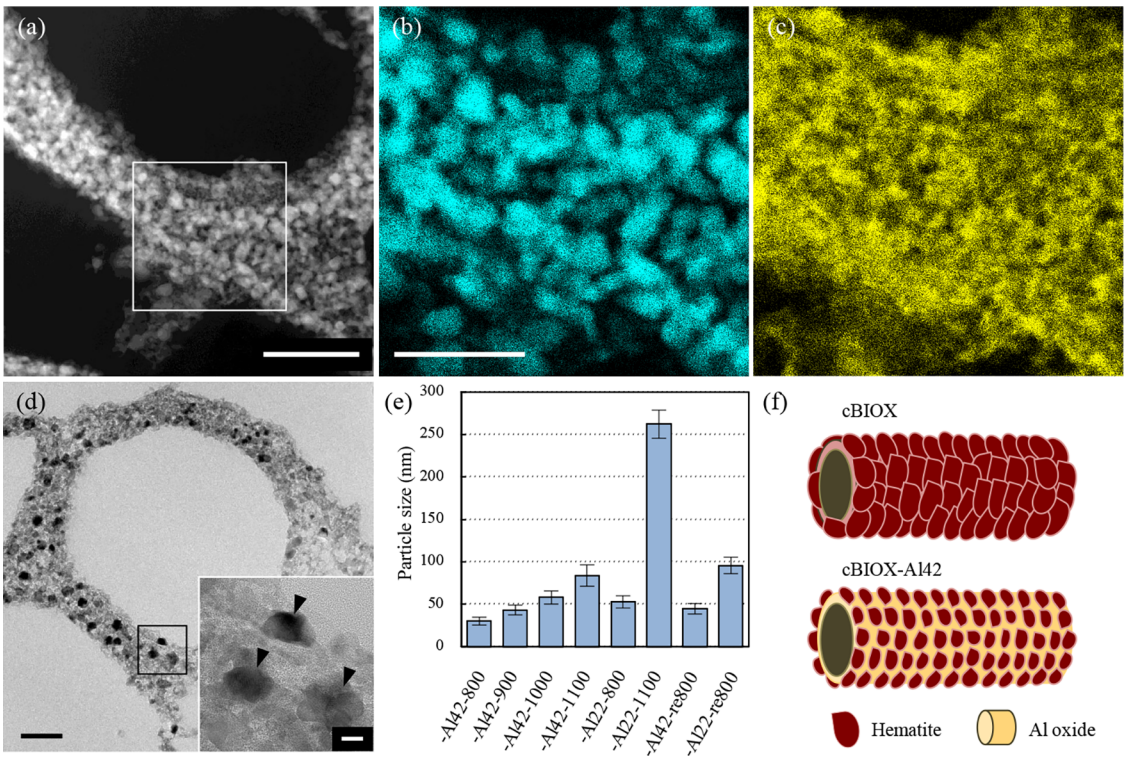

Figure 5. Microstructural analysis of and elemental distribution in cBIOX-Al sheath. (a) Dark-field STEM image of an ultrathin cross section of cBIOX-Al42 sheath. (b, c) EDS maps for (b) Fe K and (c) Al K edges corresponding to the white square area in (a). (d) TEM image of an ultrathin cross section of cBIOX-Al42 sheath. The inset is a magnified image of the black square area. Arrowheads indicate hematite particles. Scale bars are 200 nm in (a) and 100 nm in (b) and (d) (10 nm in the inset). (e) Hematite particle size (mean ± SD, n = 30) in cBIOX-Al samples after heating at the indicated temperatures (numerals after the second hyphen) or after reheating at 800 °C (re800). (f) Schematic representation of tubular nanocomposite structures of cBIOX-Al42 in comparison with a low Al-containing cBIOX sheath.

low crystalline Al oxide regions and hematite particles embedded therein. This work therefore demonstrates that the bioengineered Al-enriched BIOX can serve as an innovative high chromatic orange-hued inorganic pigment with ignorable toxicity and marked thermostability that should meet large industrial demand.

METHODS

Sample Preparation and Treatments. Al-enriched cBIOX samples were prepared using the two-step method[19] with specific modifications. Briefly, bacterial cells of *Leptothrix cholodnii* strain OUMS1 (NITE BP-860)[42] were cultured in silicon−iron−glucose−peptone liquid medium lacking an iron source (modified SIGP)[20] on a rotary shaker at 20 °C and 70 rpm for 3 days to produce the primary organic sheaths. The sheath bundles were washed twice with a 10-fold volume of Milli-Q water to remove medium constituents and bacterial soluble metabolites, immersed in a 20 mM acetate buffer (pH 4.0) supplemented with 5 mg mL^{-1} of iron powder (particle size 150 μm, Wako Pure Chemical Industries, Osaka, Japan) and were shaken at 70 rpm and 20 °C for 42 h. Then, the sulfate salt ($ZnSO_4$, $(NH_4)_2SO_4$, or Na_2SO_4 (Nacalai Tesque, Kyoto, Japan)) was added to the sheath suspension in various concentrations (1−50 mM) together with 10 mM $AlCl_3$; the suspensions were further incubated for 24 h under the same conditions. The Al-deposited BIOX sheaths were collected as precipitates, washed three times with a 10-fold volume of Milli-Q water, and freeze-dried. Heating treatments of cBIOX samples were carried out using an electric furnace at temperatures ranging from 500 to 1100 °C in increments of 100 °C for 2 h with a heating rate of 10 °C min^{-1}. Grinding treatments of cBIOX sheaths were performed using a planetary ball mill apparatus (PULVERISETTE 7, Fritsch Japan Co., Kanagawa, Japan) under conditions of three working cycles of 400 rpm for 10 min with 5 min intervals.

Analytical Characterizations. The morphology was examined by scanning electron microscopy (SEM; S-4300, Hitachi, Tokyo, Japan) and TEM (JEM-2100F, JEOL, Tokyo, Japan). Elemental analyses were performed by energy-dispersive X-ray spectroscopy (EDX; Genesis 2000, Ametek, Tokyo, Japan) coupled with S-4300, X-ray fluorescence (XRF) spectroscopy (Orbis, Ametek, Tokyo, Japan), and inductively coupled plasma-optical emission spectroscopy (ICP-OES; VISTA-PRO, Seiko Instruments Inc., Tokyo Japan). Elemental mapping images were acquired using an EDS apparatus (EX-24063JGT, JEOL, Tokyo, Japan) installed on JEM-2100F in the scanning TEM (STEM) mode with a CEOS Cs corrector. The specimens embedded in resins and ultrathin sections (~75 nm) for TEM analysis were prepared as described.[43] Crystallographic features were analyzed by powder XRD (RINT-2000, Rigaku, Tokyo, Japan) using a monochromatic Cu Kα radiation. Lattice parameters were estimated from XRD profiles using silicon as an internal standard (NIST SRM660d). The sulfate ion was analyzed by Fourier transform infrared (FTIR) spectroscopy (IRAffinity-1, Shimadzu, Kyoto, Japan) after pressing the sample (~5 mg) into a 10 mm pellet and placing it in a quartz cell with KRS-5 windows. Thermogravimetric (TG) analysis was carried out using a thermal analyzer (TG-8120, Rigaku, Tokyo, Japan). Specific surface area and pore size distribution were calculated by the

https://doi.org/10.1021/acsomega.1c07390
ACS Omega 2022, 7, 12795−12802

Brunauer–Emmett–Teller (BET) method,[44] micropore analysis (MP) method,[45] and Dollimore–Heal (DH) method[46] from nitrogen adsorption isotherms measured at −196 °C using a dedicated apparatus (BELSORP-mini-II; BEL, Osaka, Japan).

Color Measurements. Color tone values (CIE $L^*a^*b^*$) of heat-treated samples were measured by spectrophotometry (CM- 2600d, Konica–Minolta Inc., Tokyo, Japan) using a CIE standard illuminant D65 and SCI mode as previously described.[21] Powder samples were loaded into cylindrical pits (φ 8 mm, 0.5 mm in depth) on glass holders using a plastic film to flatten the compacted powders' surface for accurate measurements. A commercially available iron oxide pigment MC-55 (Morishita Bengara Kogyo Co., Ltd., Mie, Japan) was used as the color reference.

■ ASSOCIATED CONTENT

Supporting Information

The Supporting Information is available free of charge at https://pubs.acs.org/doi/10.1021/acsomega.1c07390.

Concentrations of $AlCl_3$ and $ZnSO_4$ used for cBIOX preparation and CIE Lab color values of heat-treated cBIOX-Al samples (Table S1); comparison of CIE Lab color values among cBIOX-Al samples (Table S2); morphology and chemical composition of Al-containing cBIOX samples (Figure S1); analysis of the behavior of sulfate in cBIOX-Al samples (Figure S2); crystallographic analysis of cBIOX-Al products (Figure S3); and elemental distribution analysis of cBIOX-Al42 sheath (Figure S4) (PDF)

■ AUTHOR INFORMATION

Corresponding Authors

Katsunori Tamura − *Graduate School of Natural Science and Technology, Okayama University, 700-8530 Okayama, Japan; Bengala Techno-Lab, 216-0007 Kawasaki-shi, Kanagawa, Japan;* orcid.org/0000-0002-0179-9796; Email: ktamura@okayama-u.ac.jp

Jun Takada − *Graduate School of Natural Science and Technology, Okayama University, 700-8530 Okayama, Japan*; Email: jtakada@okayama-u.ac.jp

Authors

Yuri Oshima − *Graduate School of Natural Science and Technology, Okayama University, 700-8530 Okayama, Japan*

Yuta Fuse − *Graduate School of Natural Science and Technology, Okayama University, 700-8530 Okayama, Japan*

Noriyuki Nagaoka − *Advanced Research Center for Oral and Craniofacial Sciences, Okayama University, 700-8530 Okayama, Japan*

Tatsuki Kunoh − *Graduate School of Natural Science and Technology, Okayama University, 700-8530 Okayama, Japan;* Present Address: Faculty of Life and Environmental Science, University of Tsukuba, Tsukuba, Ibaraki 305-8577, Japan; orcid.org/0000-0002-8423-2903

Makoto Nakanishi − *Graduate School of Natural Science and Technology, Okayama University, 700-8530 Okayama, Japan*

Tatsuo Fujii − *Graduate School of Natural Science and Technology, Okayama University, 700-8530 Okayama, Japan;* orcid.org/0000-0001-5343-840X

Tokuro Nanba − *Graduate School of Environmental and Life Science, Okayama University, 700-8530 Okayama, Japan*

Complete contact information is available at: https://pubs.acs.org/10.1021/acsomega.1c07390

Author Contributions

K.T. designed and directed the study and wrote the manuscript; Y.O. and Y.F. conducted sample preparations and analytical experiments; M.N. performed TG and FTIR analyses; N.N. performed TEM analysis; T.K., T.F., and T.N. provided technical advice; and J.T. developed the original concept of the project. The manuscript was reviewed by all of the authors.

Notes

The authors declare no competing financial interest.

■ ACKNOWLEDGMENTS

The authors thank Keiko Toyoda and Mika Yoneda for technical support. They are grateful to Mikio Takano and Nanao Horiishi for valuable discussion. This study was financially supported by the JST-CREST project (2012–2017) (J.T.).

■ REFERENCES

(1) Buxbaum, G.; Pfaff, G. *Industrial Inorganic Pigments*, 3rd ed.; Wiley-VCH: Weinheim, Germany, 2005.

(2) Pfaff, G. *Inorganic Pigments*; De Gruyter: Berlin, Germany, 2017.

(3) Backhaus, T.; Scheringer, M.; Wang, Z. Developing SAICM into a framework for the international governance of chemicals throughout their lifecycle: looking beyond 2020. *Integr. Environ. Assess. Manage.* **2018**, *14*, 432–433.

(4) Ahlers, J.; Stock, F.; Werschkun, B. Integrated testing and intelligent assessment-new challenges under REACH. *Environ. Sci. Pollut. Res.* **2008**, *15*, 565–572.

(5) Hulzebos, E.; Gunnarsdottir, S.; Rila, J. P.; Dang, Z.; Rorije, E. An integrated assessment scheme for assessing the adequacy of (eco)toxicological data under REACH. *Toxicol. Lett.* **2010**, *198*, 255–262.

(6) Schoeters, G. The reach perspective: toward a new concept of toxicity testing. *J. Toxicol. Environ. Health, Part B* **2010**, *13*, 232–241.

(7) Vandenberg, L. N. Reform of the toxic substances control act (TSCA): an endocrine society policy perspective. *Endocrinology* **2016**, *157*, 4514–4515.

(8) Krimsky, S. The unsteady state and inertia of chemical regulation under the US Toxic Substances Control Act. *PLoS Biol.* **2017**, *15*, No. e2002404.

(9) Yamamoto, T. The notification systems of new chemical substances in the world. *J. Imag. Soc. Jpn.* **2007**, *46*, 185–191.

(10) Jansen, M.; Letschert, H. P. Inorganic yellow-red pigments without toxic metals. *Nature* **2000**, *404*, 980–982.

(11) Mao, W.-X.; Zhang, W.; Chi, Z.-X.; Lu, R.-W.; Cao, A.-M.; Wan, L.-J. Core–shell structured Ce_2S_3@ZnO and its potential as a pigment. *J. Mater. Chem. A* **2015**, *3*, 2176–2180.

(12) Masui, T.; Takeuchi, N.; Nakado, H.; Imanaka, N. Novel environment-friendly green pigments based on rare earth cuprate. *Dyes Pigm.* **2015**, *113*, 336–340.

(13) Bae, B.; Tamura, S.; Imanaka, N. Novel environment-friendly yellow pigments based on praseodymium(III) tungstate. *Ceram. Int.* **2017**, *43*, 7366–7368.

(14) Horiishi, N. A historical survey of bengala in view of art and science. *J. Jpn. Soc. Powder Powder Metall.* **2002**, *49*, 1121–1127.

(15) MacDonald, B. L.; Stalla, D.; He, X.; Rahemtulla, F.; Emerson, D.; Dube, P. A.; Maschmann, M. R.; Klesner, C. E.; White, T. A.

Hunter-gatherers harvested and heated microbial biogenic iron oxides to produce rock art pigment. *Sci. Rep.* **2019**, *9*, No. 17070.
(16) Hashimoto, H.; Asaoka, H.; Nakano, T.; Kusano, Y.; Ishihara, H.; Ikeda, Y.; Nakanishi, M.; Fujii, T.; Yokoyama, T.; Horiishi, N.; Nanba, T.; Takada, J. Preparation, microstructure, and colour tone of microtubule material composed of hematite/amorphous-silicate nanocomposite from iron oxide of bacterial origin. *Dyes Pigm.* **2012**, *95*, 639−643.
(17) Hashimoto, H.; Fujii, T.; Kohara, S.; Asaoka, H.; Kusano, Y.; Ikeda, Y.; Nakanishi, M.; Benino, B.; Nanba, T.; Takada, J. Amorphous structure of iron oxide of bacterial origin. *Mater. Chem. Phys.* **2012**, *137*, 571−575.
(18) Kunoh, T.; Kunoh, H.; Takada, J. Perspectives on the biogenesis of iron oxide complexes produced by *Leptothrix*, an iron-oxidizing bacterium and promising industrial applications for their functions. *J. Microb. Biochem. Technol.* **2015**, *07*, 419−426.
(19) Tamura, K.; Kunoh, T.; Nakanishi, M.; Kusano, Y.; Takada, J. Preparation and characterization of additional metallic element-containing tubular iron oxides of bacterial origin. *ACS Omega* **2020**, *5*, 27287−27294.
(20) Ishihara, H.; Hashimoto, H.; Taketa, E.; Suzuki, T.; Mandai, K.; Kunoh, H.; Takada, J. Silicon-rich, iron oxide microtubular sheath produced by an iron-oxidizing bacterium, *Leptothrix* sp. strain OUMS1, in culture. *Minerals* **2014**, *4*, 565−577.
(21) Tamura, K.; Kunoh, T.; Nagaoka, N.; Takada, J. High-quality inorganic red pigment prepared by aluminum deposition on biogenous iron oxide sheaths. *ACS Appl. Bio Mater.* **2020**, *3*, 5699−5707.
(22) Asaoka, H.; Kusano, Y.; Nakanishi, M.; Fujii, T.; Takada, J. Characterization and reproduction of "Fukiya Bengara," noble red color pigment, by Fe_2O_3-Al_2O_3 system. *J. Jpn. Soc. Powder Powder Metall.* **2003**, *50*, 1062−1067.
(23) Hashimoto, H.; Nakanishi, M.; Asaoka, H.; Maeda, T.; Kusano, Y.; Fujii, T.; Takada, J. Preparation of yellowish-red Al-substituted α-Fe_2O_3 powders and their thermostability in color. *ACS Appl. Mater. Interfaces* **2014**, *6*, 20282−20289.
(24) Hashimoto, H.; Kiyohara, J.; Isozaki, A.; Arakawa, Y.; Fujii, T.; Takada, J.; Inada, H.; Takaishi, T.; Asoh, H. Bright yellowish-red pigment based on hematite/alumina composites with a unique porous disk-like structure. *ACS Omega* **2020**, *5*, 4330−4337.
(25) Hashimoto, H.; Fujii, T.; Kohara, S.; Nakanishi, K.; Yogi, C.; Peterlik, H.; Nakanishi, M.; Takada, J. Structural transformations of heat-treated bacterial iron oxide. *Mater. Chem. Phys.* **2015**, *155*, 67−75.
(26) Perraud, V.; Horne, J. R.; Martinez, A. S.; Kalinowski, J.; Meinardi, S.; Dawson, M. L.; Wingen, L. M.; Dabdub, D.; Blake, D. R.; Gerber, R. B.; Finlayson-Pitts, B. J. The future of airborne sulfur-containing particles in the absence of fossil fuel sulfur dioxide emissions. *Proc. Natl. Acad. Sci. U.S.A.* **2015**, *112*, 13514−13519.
(27) Levy, A.; Merryman, E. L.; Reid, W. T. Mechanisms of formation of sulfur oxides in combustion. *Environ. Sci. Technol.* **1970**, *4*, 653−662.
(28) Silva, R.; Cadorin, L.; Rubio, J. Sulphate ions removal from an aqueous solution: I. Co-precipitation with hydrolysed aluminum-bearing salts. *Miner. Eng.* **2010**, *23*, 1220−1226.
(29) Bennett, J. W.; Bjorklund, J. L.; Forbes, T. Z.; Mason, S. E. Systematic study of aluminum nanoclusters and anion adsorbates. *Inorg. Chem.* **2017**, *56*, 13014−13028.
(30) Kosmas, C. S.; Franzmeier, D. P.; Schulz, D. G. Relationship among derivative spectroscopy, color, crystallite dimensions and Al-substitution of synthetic goethites and hematites. *Clays Clay Miner.* **1986**, *34*, 625−634.
(31) Elias, M.; Chartier, C.; Prévot, G.; Garay, H.; Vignaud, C. The colour of ochres explained by their composition. *Mater. Sci. Eng. B* **2006**, *127*, 70−80.
(32) Popović, S.; Ristić, M.; Musić, S. Formation of solid solutions in the system Al_2O_3-Fe_2O_3. *Mater. Lett.* **1995**, *23*, 139−142.
(33) Stößer, R.; Nofz, M.; Feist, M.; Scholz, G. Fe^{3+}-assisted formation of α-Al_2O_3, starting from sol−gel precursors. *J. Solid State Chem.* **2006**, *179*, 652−664.
(34) Yanagisawa, M.; Sugiura, I.; Hotta, T.; Tsubaki, J.; Hosono, H. Discoloration of alumina ceramics with ultraviolet radiation and elucidation of its mechanism. *J. Ceram. Soc. Jpn.* **1993**, *101*, 1189−1191.
(35) Yang, S.-T.; Wang, T.; Dong, E.; Xin-Xin Chen, X.-X.; Xiang, K.; Liu, J.-H.; Liu, Y.; Wang, H. Bioavailability and preliminary toxicity evaluations of alumina nanoparticles in vivo after oral exposure. *Toxicol. Res.* **2012**, *1*, 69−74.
(36) Willhite, C. C.; Karyakina, N. A.; Yokel, R. A.; Yenugadhati, N.; Wisniewski, T. M.; Arnold, I. M. F.; Momoli, F.; Krewski, D. Systematic review of potential health risks posed by pharmaceutical, occupational and consumer exposures to metallic and nanoscale aluminum, aluminum oxides, aluminum hydroxide and its soluble salts. *Crit. Rev. Toxicol.* **2014**, *44*, 1−80.
(37) Akbaba, G. B.; Türkez, H. Investigation of the genotoxicity of aluminum oxide, β-tricalcium phosphate, and zinc oxide nanoparticles in vitro. *Int. J. Toxicol.* **2018**, *37*, 216−222.
(38) Jalili, P.; Huet, S.; Lanceleur, R.; Jarry, G.; Le Hegarat, L.; Nesslany, F.; Hogeveen, K.; Fessard, V. Genotoxicity of aluminum and aluminum oxide nanomaterials in rats following oral exposure. *Nanomaterials* **2020**, *10*, No. 305.
(39) Sadiq, R.; Khan, Q. M.; Mobeen, A.; Hashmat, A. J. In vitro toxicological assessment of iron oxide, aluminium oxide and copper nanoparticles in prokaryotic and eukaryotic cell types. *Drug Chem. Toxicol.* **2015**, *38*, 152−161.
(40) Moradi, M.; Kim, J. C.; Qi, J.; Xu, K.; Li, X.; Ceder, G.; Belcher, A. M. A bio-facilitated synthetic route for nano-structured complex electrode materials. *Green Chem.* **2016**, *18*, 2619−2624.
(41) Wu, R.; Tao, X.; Xia, Y.; Zhang, W.; et al. Biotemplated fabrication of Sn@C anode materials based on the unique metal biosorption behavior of microalgae. *ACS Appl. Mater. Interfaces* **2014**, *6*, 3696−3702.
(42) Sawayama, M.; Suzuki, T.; Hashimoto, H.; Kasai, T.; Furutani, M.; Miyata, N.; Kunoh, H.; Takada, J. Isolation of a *Leptothrix* strain, OUMS1, from ocherous deposits in groundwater. *Curr. Microbiol.* **2011**, *63*, 173−180.
(43) Suzuki, T.; Hashimoto, H.; Matsumoto, N.; Furutani, M.; Kunoh, H.; Takada, J. Nanometer-scale visualization and structural analysis of the inorganic/organic hybrid structure of *Gallionella ferruginea* twisted stalks. *Appl. Environ. Microbiol.* **2011**, *77*, 2877−2881.
(44) Brunauer, S.; Emmett, P. H.; Teller, E. Adsorption of gases in multimolecular layers. *J. Am. Chem. Soc.* **1938**, *60*, 309−319.
(45) Mikhail, R. S.; Brunauer, S.; Bodor, E. E. Investigations of a complete pore structure analysis I. Analysis of microstructure. *J. Colloid Interface Sci.* **1968**, *26*, 45−53.
(46) Dollimore, D.; Heal, G. R. Pore-size distribution in typical adsorbent systems. *J. Colloid Interface Sci.* **1970**, *33*, 508−519.

https://doi.org/10.1021/acsomega.1c07390
ACS Omega 2022, 7, 12795−12802